Imaging and suppression of Lamb modes using adaptive beamforming

2011 Smart Mater. Struct. 20 085024

(http://iopscience.iop.org/0964-1726/20/8/085024)

Smart Mater. Struct. **20** (2011) 085024 (13pp) doi:10.1088/0964-1726/20/8/085024

Imaging and suppression of Lamb modes using adaptive beamforming

Marcus Engholm, Tadeusz Stepinski and Tomas Olofsson

Uppsala University, Signals and Systems, Box 534, 751 21 Uppsala, Sweden

E-mail: marcus.engholm@gmail.com

Received 12 December 2010, in final form 1 June 2011
Published 22 July 2011
Online at stacks.iop.org/SMS/20/085024

Abstract

Lamb waves have proven to be very useful for plate inspection because large areas of a plate can be covered from a fixed position. This capability makes them suitable for both inspection and structural health monitoring (SHM) applications. During the last decade, research on the use of active arrays in combination with beamforming techniques has shown that a fixed array can be used to perform omni-directional monitoring of a plate structure. The dispersion and multiple propagating modes are issues that need to be addressed when working with Lamb waves. Previous work has mainly focused on conventional, delay-and-sum (DAS) beamforming, while reducing the effects of multiple modes through frequency selectivity and transducer design.

The paper describes an adaptive beamforming technique using a minimum variance distortionless response beamforming (MVBF) approach for spatial Lamb wave filtering with multiple-transmitter–multiple-receiver arrays. Dispersion is compensated for by using theoretically calculated dispersion curves.

Simulations are used for evaluating the performance of the technique for suppression of interfering Lamb modes, both with and without the presence of mode conversion using different array configurations. A simple simulation model of the plate is used to compare the performance of different sizes of active arrays. An aluminum plate with artificial defects is used for the experimental evaluation.

The results show that the MVBF approach performs a lot better in terms of resolution and suppression of interfering modes than the widely used standard beamformer.

1. Introduction

Guided waves in structures allow the inspection of large areas from a fixed position. Areas which are not accessible using traditional NDT methods, such as eddy current or bulk wave pulse–echo ultrasound, can potentially be inspected or monitored using guided waves. Examples of applications for guided waves are the inspection of piping [1] and plates [2].

Guided waves in plates, also known as Lamb waves, share fundamental properties with other types of guided waves, such as dispersion and the existence of multiple propagating modes. Dispersion causes the signal to spread out, which reduces the spatial and temporal resolution of the received unprocessed data, a significant issue in applications where range is to be estimated. Furthermore, Lamb modes differ in dispersion characteristics and propagate at different velocities making interpretation of backscattered signals complicated in the presence of multiple modes. Overlapping modes can make the identification of small defects and time-of-flight estimation difficult.

During the last decade the use of active Lamb wave arrays for the imaging of larger plate areas has been proposed by several authors. There are two options to achieve the directionality required for imaging applications, physical or electronic array steering. Different approaches to electronic steering, that is typically performed in post-processing, have been treated in numerous publications [3–8]. Examples of physically directional arrays include the CLoVER transducer [9], which consists of a circle of angularly directional elements, each covering an angular sector. This paper focuses on electronic steering using algorithms for post-processing of array data. One or more elements in the array generate a pulse that propagates along the plate. The backscattered signals from defects and other discontinuities are received by the array and post-processed to form an image of the reflectors in the plate. As for other guided wave

applications, reduction of interference from other modes is of major importance. Proper design of transducers used for excitation and detection in combination with careful frequency selection can significantly reduce the influence of interfering modes. Some examples presented in the field include the use of electromechanical acoustic transducers (EMAT) [5, 10] and piezoelectric transducers [6, 11]. The drawback of these approaches is that they require limited bandwidth input signals to work efficiently. Limited bandwidth leads to reduced spatial resolution since the length of the signal increases.

The effect of dispersion can be reduced by selecting a frequency region with relatively low dispersion. Wilcox showed that by using theoretically calculated dispersion curves, time domain data can be transformed into dispersion compensated spatial domain data over a wider frequency range for a single mode [5, 12].

The above cited works, in common with most other work presented in the literature concerning array processing of Lamb waves, focused on the standard beamformer (SBF). The standard beamformer is robust, easy to implement, and computationally simple. However, compared to more advanced array processing methods it suffers from poor resolution and high sidelobes. In [5] a deconvolution approach based on the theoretical point spread function was used to reduce the sidelobe level. A more general approach to beamformer design was proposed by Velichko and Wilcox in [13]. However, neither of these methods is data dependent and will therefore assume a worst case scenario: signals are assumed to impinge from all directions. This will lead to a suboptimal use of the available degrees of freedom in the beamformer. If knowledge of the actual interferers were available, an optimal beamformer could be derived to cancel interferers much more efficiently. Such beamformers are known as adaptive beamformers, and have not been extensively used in Lamb wave applications.

Adaptive beamformers have been successfully utilized in, for example, radar, sonar, and medical ultrasound applications, resulting in improved resolution and interference suppression compared to the SBF. Contrary to the SBF, an adaptive beamformer is optimized based on some data criterion, such as minimizing the influence of interfering signals in the received data. One of the most commonly used adaptive beamformers is based on the minimum variance distortionless response (MVDR) approach. Previous work on the MVDR approach in the medical ultrasound field include Wang *et al* [14], Sasso and Cohen-Bacrie [15], and Synnevåg *et al* [16]. Another, but not entirely related, approach using the MVDR method for Lamb wave processing was proposed by Michaels *et al* [17] for processing change based data from a distributed array in a tomographic setup.

In [18–21], the MVDR approach was compared to a SBF for passive direction-of-arrival (DOA) estimation of Lamb waves, which showed that the MVDR approach performs much better in terms of resolution and sidelobe level. The work was extended to a complete active imaging procedure in [21, 22], where a single transmitter and a fixed array of receivers was used to inspect a plate. The MVDR beamformer (MVBF) showed much better resolution and suppression of interfering Lamb modes compared to the SBF. Improved suppression of interfering Lamb modes may relax requirements on array element design and bandwidth of the input signals. Increasing the bandwidth of the probing pulse improves range resolution. However, the most significant drawback of the MVDR approach is its inability to handle correlated sources. This is especially true for active imaging setups, where the backscattered signals are likely to be highly correlated. Due to this, the previous approach [22], employing a single transmitter, requires certain preprocessing to achieve the desired result. This in turn puts some constraints on the geometry of the array and limits the effective aperture size.

In this paper a setup with multiple transmitters is considered. The use of multiple transmitters avoids the need for preprocessing, which enables more flexibility in array design, and can lead to improved performance compared to single transmitter setups [21]. The paper is organized as follows: the problem is stated in section 2, followed in section 3 by a short overview of the relevant properties of Lamb waves. Its implications for Lamb wave imaging are discussed in section 4. The performance of the proposed method compared to both a single transmitter setup and the SBF is evaluated in section 5. The SBF comparison considers two scenarios: first, simulation results of the mode suppression capabilities of three different array configurations are presented, followed by simulation and experimental results of a plate inspection scenario. A discussion and conclusions are given in sections 6 and 7, respectively. More background information concerning the use of the MVDR approach for Lamb waves can be found in the authors previous paper [22].

2. Problem formulation

The objective is to detect and estimate the size of defects in a plate structure by means of a 2D array capable of generating and receiving Lamb waves. Data acquired through successive excitation of transmitting elements in the array, and reception performed using all the receiving array elements, allow estimation of the reflected power in each point $\mathbf{z} = [x, y]^{\mathrm{T}}$ in an area in the vicinity of the array, the region of interest (ROI). The dispersive and multi-modal properties of the propagating Lamb waves need to be addressed to achieve adequate results. Omni-directional coverage in both near- and far-field of the array is desirable to fully utilize the array. The results presented in the paper have been acquired using uniform rectangular arrays (URAs). However, the method is not restricted to any particular array configuration.

The setup and geometrical notations are illustrated in figure 1. Let $g_{p,m}(t)$ denote the received signal for the pth transmitter and mth receiver. Each of the P transmitting elements is excited separately, but the backscattered signals are received by all M receiving elements either simultaneously or multiplexed through repeated transmitter excitation. The approach is general in the sense that either an active array (pulse–echo mode) or a combination of transmitting and receiving arrays (pitch–catch) can be considered. It is assumed that $g_{p,m}(t)$ is an analytic (complex) signal, hence, all negative frequency components are zero.

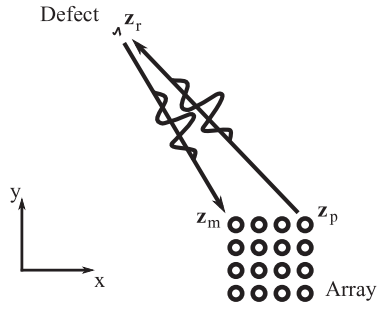

Figure 1. A 4×4 rectangular active array with current transmitter $\mathbf{z}_p$ and receiver $\mathbf{z}_m$. A defect is assumed to be present at $\mathbf{z}_r$.

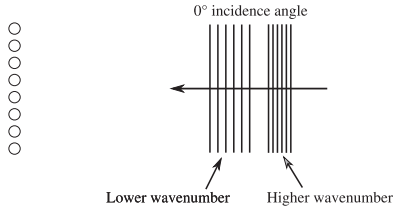

Figure 2. Two Lamb modes with different wavenumber impinging on a ULA.

3. Theoretical background

3.1. Lamb waves

3.1.1. Lamb modes. To perform imaging using Lamb waves over a wide frequency band, the dispersive properties of the Lamb waves need to be addressed. A necessary step in both simulation and compensation of dispersion is the estimation of the theoretical dispersion characteristics of the monitored structure. If accurate estimates of the material properties of the object are available, the dispersion characteristics can be determined by solving the Rayleigh–Lamb frequency equations [23]. Another possibility is to experimentally estimate the dispersion using, for example, the 2D fast Fourier transform (FFT) approach proposed by Alleyne and Cawley [24]. This can be particularly valuable for complex structures, and for evaluating the response of the array elements in terms of mode excitation.

Depending on the frequency of the signal and the thickness of the plate, the number of Lamb modes may range from two to infinity. The Lamb modes are named S_0, S_1, ... for symmetric modes, and A_0, A_1, ... for antisymmetric modes. In the following sections a simple index, $n = 0, 1, 2, 3, \ldots$, is used to identify modes S_0, A_0, S_1, A_1, ... The wavenumber for the frequency ω of the nth mode is denoted $k_n(\omega)$.

3.1.2. Directionality of arrays. Arrays are commonly used as spatial filters enabling directional resolution. One-dimensional (1D) arrays, such as uniform linear arrays (ULA), where all array elements are uniformly distributed on a line, offer at best 180° azimuthal coverage. Furthermore, the performance of a ULA in terms of angular resolution is highly dependent on the azimuth. Two-dimensional (2D) arrays on the other hand offer 360° azimuthal coverage. Examples of the most common 2D array configurations are circular and rectangular arrays.

For Lamb waves, array steering is performed by matching the phase shifts corresponding to a particular mode's dispersion characteristics for a given frequency. This is modeled using the so-called array steering vector. The signals from the array elements are aligned to coherently sum signals matching a selected direction and mode. Other modes and directions will not add up constructively, which will result in their suppression.

Beamforming of broadband signals is performed either in time domain, where delays are used to align the signals from a particular direction, or by processing each frequency component separately and superimposing the results.

3.1.3. Mode suppression. Besides dispersion, the interference from multiple propagating modes creates difficulties when interpreting Lamb wave measurement data. The backscattered signal from a defect can consist of multiple dispersed modes arriving at different times, which could be misinterpreted as defects, overlap weaker defects, and make time-of-flight estimation difficult.

As discussed earlier, a 2D array is required for 360° coverage, but as will be explained below, 2D arrays offer another advantage over 1D arrays which is highly relevant for Lamb waves.

Consider two different overlapping plane wave Lamb modes impinging on a ULA from 0°, as illustrated in figure 2. The modes have different wavenumbers and propagate at different velocities. Unless there is *a priori* information available concerning the shape and propagation of the modes, these are obviously impossible to separate for any beamformer. The reason is that all the array elements are at approximately the same distance from the source, in other words, all modes have the same steering vector for this angle: the unit vector $\mathbf{1}$. A 2D array, on the other hand, allows separation since its elements are at different distances from the target and non-focused modes will therefore not add up coherently. SBFs rely completely on this concept which, to work efficiently, requires relatively many array elements. The benefit of using an adaptive beamformer is that they allow much more efficient use of the limited array size. Examples illustrating this are presented in section 5.

3.1.4. Mode conversion. When a Lamb wave is reflected or transmitted at a boundary, some of the energy of the particular incoming Lamb mode may be converted into other modes. Depending on the characteristics of the boundary and the frequency content of the impinging Lamb wave, the conversion could occur between modes of different order, e.g. A_0 to A_1, as well as between antisymmetric and symmetric modes [23]. Thus, a signal received as a particular mode may be the result of another mode propagating from the transmitting transducer to the boundary at a different velocity. A few simulation examples featuring mode conversion will also be presented in section 5.

3.1.5. Simulation model. To enable evaluation of the MVBF compared to the SBF under ideal conditions, a simplified

simulation model has been used. The model simulates multiple reflections of two propagating modes impinging on the array, the S_0 and A_0 modes.

In practice, the excitation of a particular mode depends both on the transducer and the excitation frequency. Here it is simply assumed that both modes have been excited and the resulting out-of-plane surface displacement is $T(\omega)$ for both modes. Further assume that there are R point scatterers in the plate that scatter incident waves equally in all directions and that no secondary scattering occurs. The transmitting elements $p = 1 \cdots P$ act as omni-directional point sources, and are excited individually. Let $G_{p,m}(\omega)$ denote the signal received by array element m from an excitation of transmitter p. The received signals from a scatterer are given by the sum of the two modes and the corresponding phase shifts due to dispersion in the path from the transmitting array element p, to the reflector r, and back to the receiving element m. The resulting signals are superpositions of the contributions from the R reflectors

$$G_m(\omega) = \sum_{r=1}^{R} \sum_{n=0}^{1} \frac{1}{\sqrt{z_{r,p} z_{r,m}}} R_{r,n} T(\omega) \mathrm{e}^{-\mathrm{j}k_n(\omega)(z_{r,p}+z_{r,m})} \quad (1)$$

where the distances $z_{r,p} = \|\mathbf{z}_r - \mathbf{z}_p\|$ and $z_{r,m} = \|\mathbf{z}_r - \mathbf{z}_m\|$ are the scatterer–transmitter and scatterer–receiver distance, respectively, and $\mathbf{z}_r$, $\mathbf{z}_m$, and $\mathbf{z}_p$, shown in figure 1, are the positions of the scatterer, the receiver, and the transmitter, respectively. The frequency independent reflection coefficient for reflector r and mode n is denoted $R_{r,n}$. The first factor in (1) is due to the divergence of the cylindrical waves from the point sources and point scatterers.

For the case with mode conversion, where some of the power of mode n is converted into another mode n' at the reflector, the expression in the sum (1) becomes

$$R_{r,nn'} T(\omega) \mathrm{e}^{-\mathrm{j}(k_n(\omega) z_{r,p} + k_{n'}(\omega) z_{r,m})} \quad (2)$$

where $R_{r,nn'}$ is the amplitude of the converted mode at reflector r, and $k_{n'}(\omega)$ the wavenumber of mode n'.

3.2. Minimum variance distortionless response beamformer

Contrary to the SBF, the MVBF beamformer is capable of adaptive suppression of interfering signals and modes. To achieve this it requires information on the noise and interference environment in the form of the spatial covariance matrix, denoted $\mathbf{R}$. The elements of the spatial covariance matrix are the interelement covariance estimates of the signals received by the array. The estimation of the covariance matrix is the most critical step in the MVDR approach and its accuracy has significant impact on the final result.

The MVBF in its standard form, similar to many other advanced array processing methods, assumes narrowband signals. Furthermore, it is not able to separate backscattered signals, since they are typically correlated, which may result in so-called signal cancelation [25]. This manifests itself as the suppression and spatial perturbation of the relevant signal by the beamformer. Another major disadvantage of the MVBF is that it is sensitive to errors in the steering vector, where even small errors can lead to suppression of the desired signal [26]. The following sections will address those issues.

4. Methods

Generally, there are two ways of obtaining high range resolution in imaging: either using short pulses or long pseudo-random sequences. The first, which is most commonly used in ultrasonic imaging, requires the transmission of broadband signals that, when scattered, are received by the array elements. However, many array processing methods, such as MVBF, are formulated for narrowband signals. Thus, the most straightforward and most commonly used approach to handle broadband signals is to perform the estimation for each frequency separately using the frequency domain version of the covariance matrix, that is, the spectral matrix. The drawback of such an approach is that the correlation between different frequencies of the signal is not utilized. Additionally, a poor signal-to-noise ratio (SNR) leads to high variance in the estimates of the individual narrowband spectral matrices [27]. Furthermore, since broadband signals are typically limited in time there is a trade-off between the frequency resolution and the number of snapshots used for averaging, which also has a negative impact on the individual spectral matrix estimates. To utilize the broadband nature of the signal a number of preprocessing procedures have been proposed in the literature, for example the coherent subspace approach [28] and the steered covariance matrix [27].

Signal cancelation can be reduced by using, for example, spatial smoothing [29], which decorrelates the signals and also reduces the variance of the estimated covariance matrix. Spatial smoothing can only be applied on arrays with regular geometries that can be divided into a set of identical subarrays. This process reduces the effective aperture size to that of the subarray.

The decorrelating preprocessing step is necessary in passive scenarios, and for setups consisting of only one transmitter. In [22], using only a single transmitter, this was performed using spatial smoothing. This requires the array to be divided into subarrays. For each subarray a covariance matrix is estimated. The covariance matrices for the subarrays are then averaged to perform the so-called spatial smoothing. The drawback with this approach is that effective aperture size is reduced to the size of the subarrays. For active array setups, where each element can be excited separately, this problem is avoided. The multiple and slightly different snapshots created by the separate element excitations have the same effect as the subarray averaging of the spatial smoothing approach [30], without the reduction in effective aperture size. For setups having significantly fewer transmitters than receivers, a combination of multiple transmitters and spatial smoothing may be considered. A comparison between a single transmitter setup using spatial smoothing and a multiple transmitter setup is given in section 5.

4.1. Steered pseudo-covariance matrix

To take advantage of the bandwidth of broadband signals, the steered covariance matrix approach was introduced by Krolik [27] for far-field broadband source localization. The idea is to pre-steer the data before estimating the covariance matrix. What is gained by doing so is that all frequency

components of a potential broadband signal from the steered direction will have a unit steering vector, **1**, which allows for direct application of MVDR to calculate a broadband adaptive weight vector.

The basic concept of this approach has been applied on near-field data for adaptive beamforming of linear arrays in medical ultrasound by Wang [14] *et al*, Sasso and Cohen-Bacrie [15] and Synnevåg *et al* [16]. In this work the approach is extended to 2D arrays and dispersive signals.

For non-dispersive signals, such as those in the acoustical environment of medical ultrasound, the steering of the received signals prior to calculation of the covariance matrix is performed using time delays. Using delays for broadband dispersive Lamb waves will not lead to coherent alignment of the signals since the frequency components propagate at different phase velocities. In the same manner as [22], the alignment is obtained by backpropagating the signal $g_{p,m}(t)$, for a particular mode n, as [12]

$$h_{p,m,n}(\mathbf{z}) = \sqrt{z_{r,p} z_{r,m}} \sum_{\omega_s} G_{p,m}(\omega_s) \mathrm{e}^{jk_n(\omega_s)(z_{r,p}+z_{r,m})} \tag{3}$$

where $G_{p,m}(\omega_s)$ is the Fourier transform of the received signal, $g_{p,m}(t)$, p denotes the transmitter, and $z_{r,p} = \|\mathbf{z}_r - \mathbf{z}_p\|$ and $z_{r,m} = \|\mathbf{z}_r - \mathbf{z}_m\|$. The first factor compensates for the divergence and the exponential introduces the proper phase shift to compensate for the dispersion and propagation.

The procedure only compensates for the dispersion and propagation of one mode. Other modes are not aligned. In the sequel it is assumed that a particular mode is selected, hence the mode index, n, is dropped for notional convenience. To avoid spatial aliasing the frequencies used in (3) should be limited so that the minimum wavelength for any mode is more than twice the element distance in the array. Assuming that $g_{p,m}(t)$ is a complex (analytical) signal, spectral components above the Nyquist frequency in the discrete Fourier transform are zero. Note that there is a risk that other modes wrap-around due to the phase shifts; in such cases the received signals should be zero-padded before processing.

Potential wave attenuation is not compensated for since it is assumed to be small. However, if the attenuation is significant and known, it is straightforward to include a compensating factor in (3).

To estimate the reflected power from a focus point $\mathbf{z}$, the received signals from all array elements are phase-shifted according to (3) to compensate for the propagation and dispersion corresponding to the distance between the transmitter p, the focus point $\mathbf{z}$, and the receiver m. This results in a focused vector

$$\mathbf{h}_p(\mathbf{z}) = [h_{p,1}(\mathbf{z}) h_{p,2}(\mathbf{z}) \cdots h_{p,M}(\mathbf{z})]^{\mathrm{T}}, \tag{4}$$

for each transmitter p. A rank one covariance matrix for transmitter p is formed as

$$\widehat{\mathbf{R}}_p(\mathbf{z}) = \mathbf{h}_p(\mathbf{z}) \mathbf{h}_p^{\mathrm{H}}(\mathbf{z}). \tag{5}$$

In order to get a proper estimate of the covariance matrix it is necessary to have several snapshots. One option is to average over nearby points. However, since broadband signals are considered, which will be spatially confined around the actual scatterer, this may not improve the estimate. A better approach is to utilize the multiple snapshots acquired over the successive transmitter excitations. In addition to improving the estimate of the covariance matrix, it will lead to a decorrelation of the backscattered signals, which was discussed at the beginning of this section.

Let the matrix $\mathbf{H}(\mathbf{z})$ be defined as

$$\mathbf{H}(\mathbf{z}) = [\mathbf{h}_1(\mathbf{z}) \mathbf{h}_2(\mathbf{z}) \cdots \mathbf{h}_P(\mathbf{z})]. \tag{6}$$

The focused covariance matrix can then be estimated as the average of all rank 1 covariance matrices from each transmitter, $\mathbf{h}_p(\mathbf{z})\mathbf{h}_p^H(\mathbf{z})$, as

$$\hat{\mathbf{R}}(\mathbf{z}) = \frac{1}{P} \mathbf{H}(\mathbf{z}) \mathbf{H}^H(\mathbf{z}). \tag{7}$$

Thus, each point in the ROI requires a separate covariance matrix which results in more computational effort compared to a conventional covariance matrix. The advantage, however, is that this approach enables processing of dispersed near-field broadband signals which is not possible with the standard MVDR approach.

4.2. MVBF

Since the proper phase shifts for steering and dispersion compensation for each frequency are already applied in the steered covariance matrix $\hat{\mathbf{R}}(\mathbf{z})$, the steering vector for point $\mathbf{z}$ takes simply the form of the unit vector **1**, which results in the following MVBF weight vector

$$\mathbf{w}(\mathbf{z}) = \frac{\hat{\mathbf{R}}^{-1}(\mathbf{z})\mathbf{1}}{\mathbf{1}^{\mathrm{T}}\hat{\mathbf{R}}^{-1}(\mathbf{z})\mathbf{1}}. \tag{8}$$

Note that if the number of transmitters P is less than the number of receivers M, the covariance matrix (7) will be non-invertible. This will be addressed in section 4.4.

The weight vector $\mathbf{w}(\mathbf{z})$ is then applied on the received signals from each excitation and the outputs are subsequently averaged

$$y(\mathbf{z}) = \frac{1}{P} \sum_{p=1}^{P} \mathbf{w}^{\mathrm{H}}(\mathbf{z}) \mathbf{h}_p(\mathbf{z}). \tag{9}$$

The backpropagation step in (3) has already aligned the signals for the particular mode, making the SBF output simply the average of the focused signals

$$y(\mathbf{z}) = \frac{1}{P} \sum_{p=1}^{P} \mathbf{1}^{\mathrm{H}} \mathbf{h}_p(\mathbf{z}). \tag{10}$$

Apodization can be applied to the SBF by replacing the unit vector by a suitable weight vector.

The steering vector for the steered covariance matrix is constructed with an assumption of equal amplitude over the array elements for the signal of interest. This assumption will affect the behavior of the MVBF approach compared to the SBF in the presence of near-field defects that reflect the transmitted waves in a way that leads to significantly different

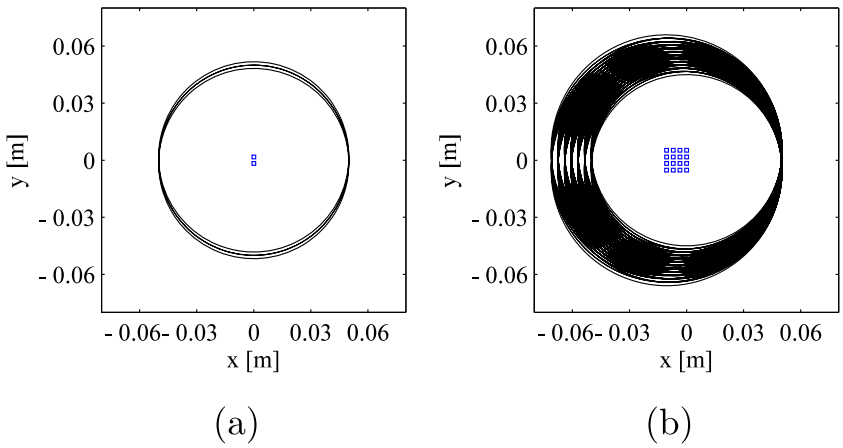

Figure 3. Elliptic focusing regions for 2 × 1 (a) and 4 × 4 (b) array.
(This figure is in colour only in the electronic version)

amplitudes over the array elements. This could typically occur when a defect is oriented in such a way that the reflected energy only reaches some array elements. The SBF will simply produce an output based on the average over the array, while the MVBF could in the worst case cancel the signal. The diagonal loading approach described below will to some degree increase the MVBF's tolerance to such signals.

4.3. Focusing regions

When performing the focusing operation for each element pair $h_{p,m,n}(\mathbf{z})$, (i.e. transmitter–receiver and receiver–transmitter), the focused range forms an ellipse intersecting the focus point $\mathbf{z}$, where the elements are located in the focal points of each ellipse. Each pair of elements forms a different ellipse, which leads to the problem that the focused signals from different element pairs can potentially contain contributions from different defects. Furthermore, because of the different angles between the transmitters, the scatterers, and the receivers it is possible that a single interfering defect spreads out spatially, which limits the performance of the MVBF. Therefore, the near-field covariance matrices, $\widehat{\mathbf{R}}_p(z)$, from each transmitter p, are not realizations of the same interference environment, which calls for a more appropriate name, a pseudo-covariance matrix. Two examples of such ellipses are illustrated in figure 3.

Although each transmission improves the estimate of the covariance matrix close to the point in focus, the resulting data could include more interferers that could actually reduce the performance of the MVBF. The MVBF is most efficient when there are only a few spatially confined interferers. When the number of interferers increases, the adaptive performance is reduced. This effect can be seen in the simulation results.

Since this issue is aggravated by an increase in the number of transmitters used for averaging in (7), one approach to mitigate the problem is to divide the transmitters into L subarrays and perform the estimation using each transmitting subarray l separately. Thus, a weight vector $\mathbf{w}_l(\mathbf{z})$ is calculated using a covariance matrix estimate from only a subset of the transmitters. The outputs, using received data and the weights from the covariance matrix estimates of each subarray, are then averaged

$$y(\mathbf{z}) = \sum_{l=1}^{L} y_l(\mathbf{z}). \tag{11}$$

4.4. Robustness and rank issues

It is well known that steering vector errors, caused by for example array calibration errors, can have a severe effect on the estimate of the MVDR algorithm [26]. This can cause the resulting weight vector to suppress the actual signal instead of the intended unit gain. Using the same approach as in [16, 22], the robustness is increased through diagonal loading

$$\widehat{\mathbf{R}}_{\text{load}} = \widehat{\mathbf{R}} + \alpha \mathbf{I} \tag{12}$$

with

$$\alpha = \frac{1}{\epsilon M} \operatorname{tr}\{\widehat{\mathbf{R}}(\mathbf{z})\} \tag{13}$$

where ϵ scales the amount of loading and tr{} is the trace. The increase in robustness comes at the cost of lower adaptivity. The diagonal loading also makes the MVBF less sensitive to differences in amplitude over the array caused by directional near-field defects.

Another issue which is common in practical applications is that the covariance matrix does not have full rank or is poorly conditioned. Rank deficiency occurs, for example, when the number of transmitters is less than the number of receivers. Sufficient diagonal loading ensures that the pseudo-covariance matrix is well conditioned.

4.5. The algorithm

The previous sections explained in detail the proposed method. The whole procedure can be summarized in the following steps performed for each point $\mathbf{z}$ in the region of interest and for a particular Lamb mode n:

(i) Compensate for dispersion using the dispersion characteristics of mode n, $k_n(\omega)$ (3).

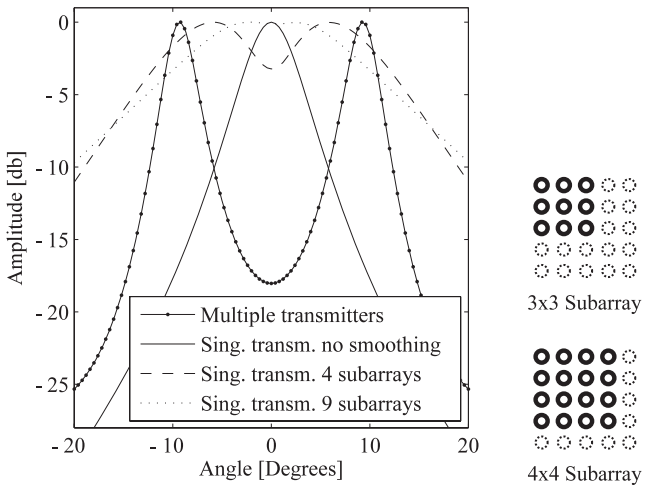

Figure 4. Left: performance comparison between the multiple transmitter approach and different single transmitter configurations using a 5 × 5 URA. Right: the subarrays used for the example: the top figure shows one of the 3 × 3 element subarrays and the bottom figure shows one of the 4 × 4 element subarrays.

(ii) Create a focused vector for point **z** (6).
(iii) Calculate the averaged covariance matrix (7).
(iv) Apply diagonal loading (12) and (13).
(v) Calculate the MVBF weight vector and estimate the power (8) and (9).

Forming a dispersion compensated SBF only requires steps 1 and 2 and its output estimate is then given by (10).

5. Results

The results are separated into two parts, a simulation study comparing the current approach to spatial smoothing and evaluating the mode suppression capabilities of the proposed method compared to the dispersion compensated SBF. Finally, both simulated and experimental results are used to compare the imaging performance of the MVBF and SBF. Discussions and conclusions concerning the results are given in subsequent sections.

5.1. Advantages over spatial smoothing

Preprocessing using spatial smoothing as performed in [22] requires certain design considerations in the trade-off between the decorrelation effect and the resolution. To demonstrate how the single transmitter approach in [22] affects the accuracy and resolution compared to a multiple transmitter setup, a 5 × 5 element URA is used in a simulation example. This array is slightly smaller than the arrays used in the other examples to illustrate the drawbacks of the single transmitter setup, which become more apparent for small arrays than for large arrays. For the single transmitter case only the center element of the first row is used for excitation, while all elements are used for the multiple transmitter case. Two scatterers, 20° apart and 0.3 m from the center of the first row of the array, reflect the transmitted waves. Figure 4 shows the result from the simulation. Three examples of a single transmitter case are shown illustrating the effects from the decorrelation step. Without spatial smoothing the two scatterers appear as a single scatterer. Dividing the array into four overlapping quadratic subarrays, with 4 × 4 elements in each subarray, resolves the two scatterers but underestimates the angle between them. With nine overlapping quadratic subarrays, having 3 × 3 elements in each subarray, both the resolution and angle estimates become very poor. To the right in figure 4 one of the subarrays from each example is shown. From the figure it can be seen that using multiple transmitters results in superior resolution and scatterer separation.

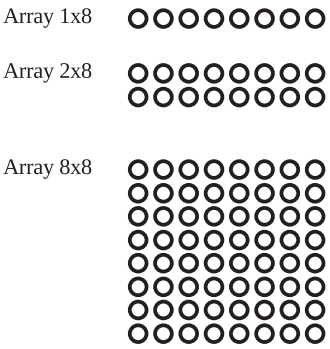

Figure 5. Array configurations used for mode suppression evaluation.

5.2. Mode suppression

The mode suppression performance of the SBF and MVBF was evaluated using simulated datasets from the three different, fully active, array configurations illustrated in figure 5. The array configurations are subsets of the 8 × 8 array, where the 1 × 8 and 2 × 8 are the top rows of the larger array. The datasets were generated using the model in section 3.1.5 with the dispersion characteristics of the 6 mm aluminum plate in section 5.3.

Two Lamb modes were simulated, the A_0 and S_0 modes, which were reflected on a single reflector located 375 mm from the center of the 8 × 8 array. Both modes were reflected with unit reflection coefficient. All array elements were excited sequentially and the backscattered signals were calculated for each array element. The element spacing was 3.5 mm, which was approximately half the minimum wavelength of the A_0 mode in the frequency range used. The input signal was a one-cycle 300 kHz sinusoid which was bandpass filtered to a bandwidth of 260 kHz. No apodization was applied on the SBF.

In the first example no mode conversions were simulated. The focusing was performed using the A_0 and S_0 mode dispersion characteristics. The results obtained using a single eight-element linear array, a 2 × 8 array and the full 8 × 8 array when focusing on the A_0 and S_0 mode are presented in figures 6 and 7, respectively. In the frequency range of the simulated signals, the A_0 mode is only slightly dispersive. By contrast, the S_0 mode is highly dispersive, which can be seen

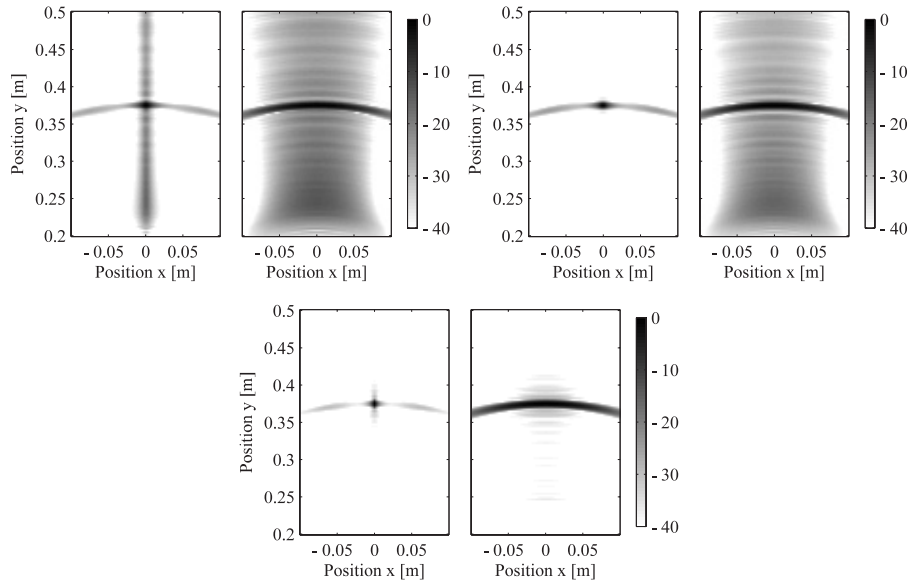

Figure 6. Simulated results illustrating the capability of suppressing the S_0 mode when focusing on the A_0 mode of reflected $S_0 - A_0$ modes using 1×8, 2×8 and 8×8 arrays. MVBF (left) and SBF (right) in each pair. The MVBF performs well using only two rows.

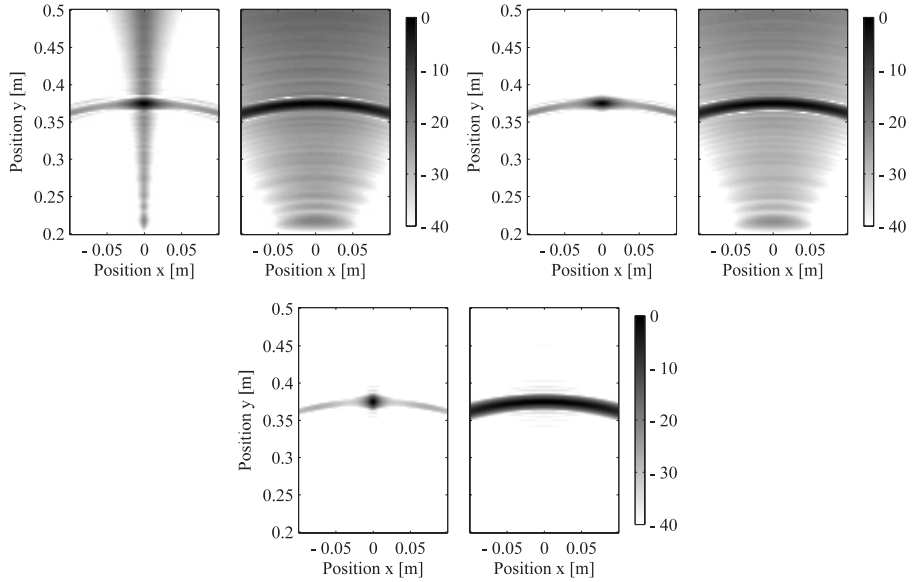

Figure 7. Simulated results illustrating the capability of suppressing the A_0 mode when focusing on the S_0 mode of reflected $S_0 - A_0$ modes using 1×8, 2×8 and 8×8 arrays. MVBF (left) and SBF (right) in each pair.

in figure 6 where it is smeared over a wide range. In figure 7 the dispersion compensation of the S_0 has the reverse effect on the A_0 mode; it becomes dispersed.

The second example evaluates the suppression capabilities of the compared methods when including mode conversion in the simulation. The same array configurations as in the previous results were used but this time a single reflection caused mode conversion between the S_0 and A_0 modes. Figure 8 shows the results for the three array configurations of two reflected modes. The S_0 mode was converted into a S_0 and an A_0 mode, where the power was divided equally between both modes. For simplicity the A_0 mode was assumed to result in a pure A_0 mode on reflection.

5.3. Plate imaging

The plate imaging evaluations were performed on a 6 mm thick, 750 × 750 mm aluminum plate (6082-T6). A number of artificial defects were created on the plate: pairs of drilled through holes, a 1 cm wide notch, and some artificial pits with depths of 1–3 mm. The layout of the defects and the positions of the receiving and transmitting arrays are shown in figure 9. The pairs of holes are labeled A, B, and C. Pair A consists of two holes, 7 mm in diameter, 28 mm apart while pairs B and C consist of two 5 mm holes each, located 21 and 10 mm apart, respectively.

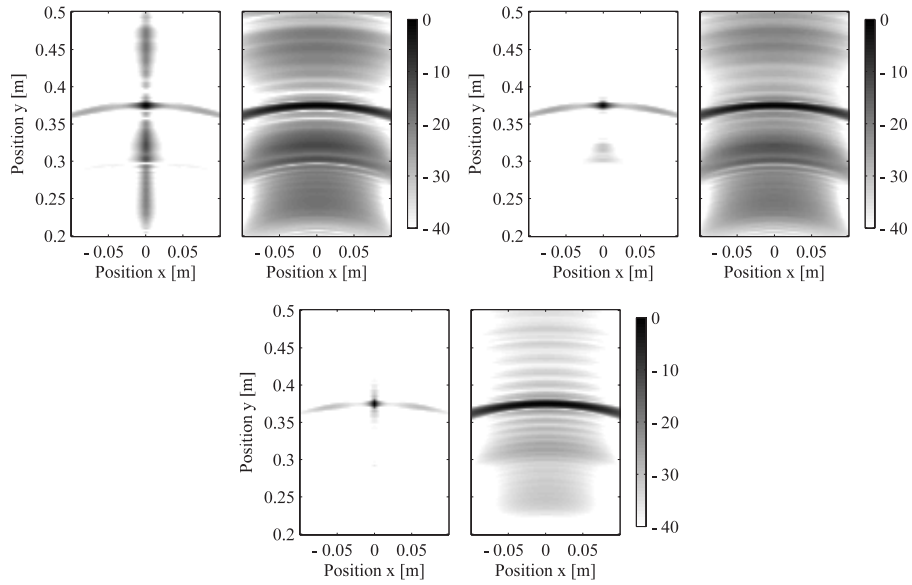

Figure 8. Simulated results of suppression capabilities of the S_0 mode and mode converted $S_0 - A_0$ mode when focusing on the A_0 mode using 1×8, 2×8 and 8×8 arrays. MVBF (left) and SBF (right) in each pair. Again, the MVBF performs very well compared to the SBF.

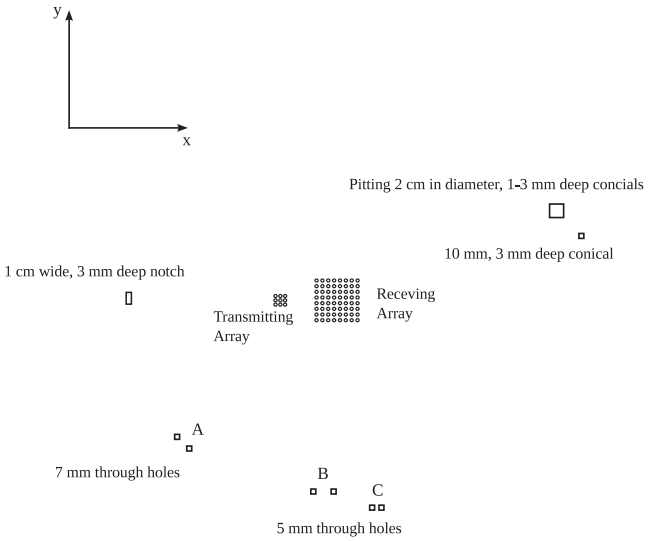

Figure 9. Layout of the aluminum plate. The labels A, B, and C identify three pairs of closely spaced holes.

The frequency range used when processing the backscattered signals was limited to 50–450 kHz, which allows the existence of three Lamb modes, the A_0, S_0, and A_1 modes, and the fundamental horizontal shear mode, SH_0. Due to the transducer's axi-symmetrical excitation and liquid coupling, the contribution from the SH_0 mode was expected to be negligible. Because of its shorter wavelength, which allows for higher resolution, the A_0 mode was selected for this scenario. The dispersion curves of the aluminum plate were determined experimentally by performing a 2D FFT of a broadband signal on a range of distances from the transmitter [24]. The resulting frequency–wavenumber plot showed significant excitation and reception of both the S_0 and A_0 modes. However, the A_1 mode was not detected in the frequency range. The longitudinal and shear wave velocities were tuned manually until good agreement between the theoretically and experimentally determined dispersion curves was achieved for the A_0 mode. The tuning resulted in a longitudinal wave velocity of 6198 m s^{-1} and a shear wave velocity of 3158 m s^{-1}. The images were formed using a grid of points, 2 mm apart. No interpolation was performed between the grid points.

The experimental setup did not allow array elements to work as both transmitters and receivers. This required a separate transmitting array, as illustrated in figure 9. Furthermore, a limited number of available transducers used as array elements required the acquisition to be performed by manual repositioning of a single transmitter and a reduced number of receivers. This will be described in detail below. The simulations are naturally not limited by this and could therefore be performed assuming a fully active array setup where all array elements acted as both transmitters and receivers.

5.3.1. Simulation results. Again, the simplified simulation model in section 3.1.5 was used along with the estimated dispersion characteristics to create datasets, here for three different active array sizes, a 4×4, a 6×6, and an 8×8 rectangular array, positioned at the center of the plate in the geometrical setup in figure 9. Only the holes, edges, and corners, were included and were simulated as point scatterers, with a positive real frequency independent reflection coefficient proportional to the diameter of the holes. For simplicity, the edge and corner reflections were also simulated as point scatterers, with reflection coefficients 10 times that of the smallest holes. It was also assumed that there was no multiple scattering or mode conversion. Using full simulated datasets of transmitter–receiver combinations figures 10, 11 and 12 show the resulting images for the active uniform rectangular arrays. No apodization was applied on the SBF.

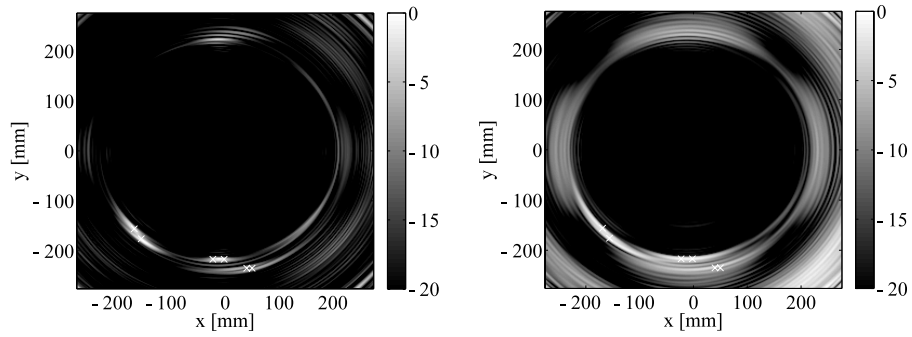

Figure 10. Simulated results using a 4 × 4 array: MVBF (left) and SBF (right).

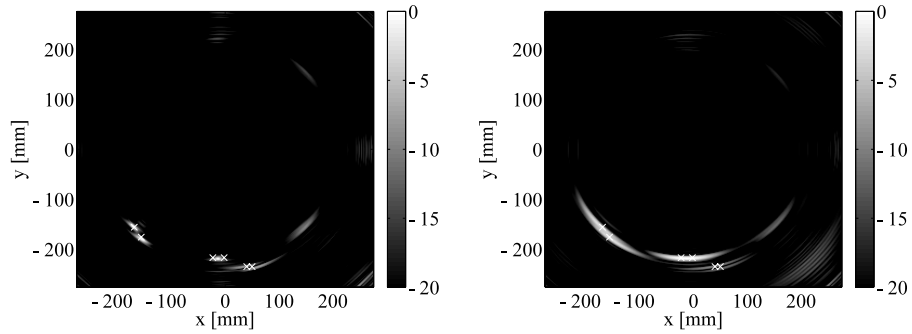

Figure 11. Simulated results using a 6 × 6 array: MVBF (left) and SBF (right).

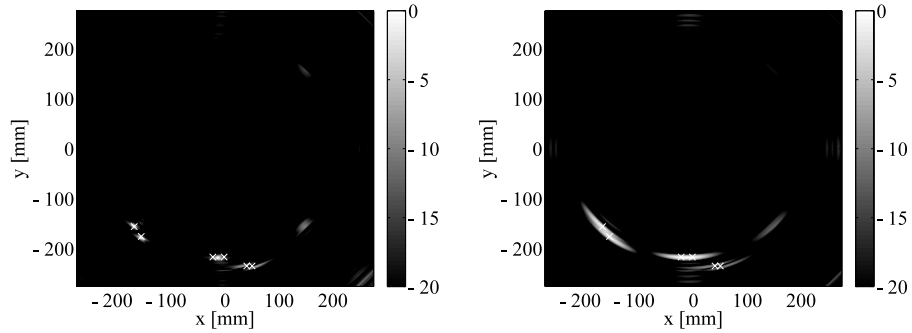

Figure 12. Simulated results using a 8 × 8 array: MVBF (left) and SBF (right).

Since the focusing was performed using the A_0 mode dispersion characteristics, the interfering dispersed S_0 mode from edge and corner reflections can be seen at even 45° angles, particularly for the 4 × 4 array. The larger arrays yield higher resolution and weaker S_0 mode, which is to be expected. Hole pair B was not resolved by any of the arrays. A false echo can be seen in the lower right quadrant of the images. It is not caused by aliasing, but is due to the combined contributions from the defects and the corner reflected S_0 mode. This is related to the discussion on focusing effects in section 4.3 above, and will be discussed in section 6.

The MVBF was not capable of suppressing the false echo, and even though it appears less smeared than that for the SBF, it has, at least relatively, slightly higher amplitude. The problem could be reduced by using only a subset of the transmitters in each covariance matrix estimate.

If no reciprocity between the transmit–receive pairs is assumed, the 8 × 8 array will produce 64 × 64 combinations. The 8 × 8 array was divided into four 4 × 4 non-overlapping transmit subarrays. Using only the transmitters from each subarray for estimation lead to four sets of 16 × 64 received signals. This results in four weight vectors calculated using the covariance matrices from each transmitting subarray. The outputs from the array using the different weight vectors were then averaged. The results from the procedure are shown in figure 13.

5.4. Experimental results

The transducers used as transmitting and receiving elements in the arrays were pinducers from Valpey Fisher Corp. The pinducers had a diameter of 1.5 mm and a resonance frequency

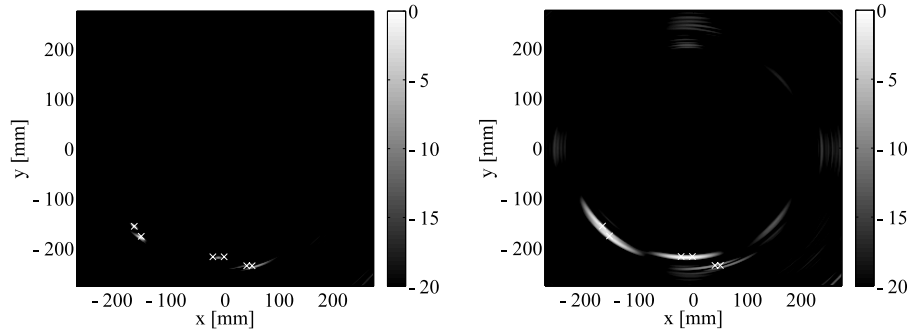

Figure 13. Simulated results using an 8 × 8 array with four transmitter subarrays: MVBF (left) and SBF (right).

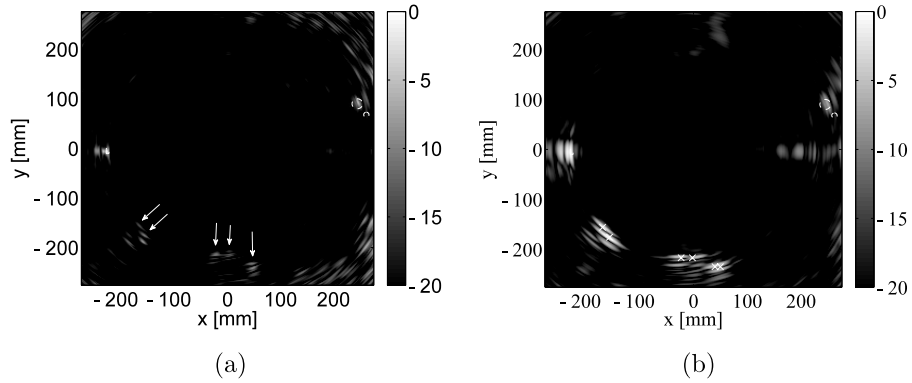

Figure 14. Measurement results from a 6 mm plate, $\epsilon = 20$: MVBF (a) and DAS (b) focusing on the A_0 mode. True positions of the defects are indicated by white crosses (holes, lower part of the image), and dashed lines (pittings and notch, at 0° and 180°, respectively). In the MVBF results, the holes are indicated by arrows to improve visibility. Log scale cut at −20 dB.

of 1.1 MHz, which was well above the frequency range used in the results yielding an approximately linear phase response in the frequency range of interest. The pinducers were coupled to the plate through a thin layer of oil which limited the detection and generation to out-of-plane displacement. To limit the influence of spatial aliasing, the element spacing in the array should be no larger than 3.5 mm. However, the shape of the pinducers allowed a minimum element distance of 7 mm, which is comparable to the minimum wavelength of the A_0 mode. Furthermore, limitations in the number of available pinducers and the electronics allowed only an eight-element linear array and a single transmitter to be used simultaneously in the setup. Thus, the measurements had to be repeated with the transmitting transducer at nine different positions, and the backscattered signal received by the eight-element linear array at eight different positions for each transmitter position. This simulated a 3 × 3 rectangular transmitting array with 3.5 mm element distance, and an 8 × 8 receiving array with 7 mm element distance, as seen in figure 9. The distance between the array centers was 50.5 mm. Since the element spacing in the receiving array by far exceeded half the minimum wavelength of the signals, aliasing effects could be expected in the experimental results. The reason for using smaller spacing between the elements in the transmitting array was to reduce the risk of near-field effects (cf section 4.3).

The input signal, a single square pulse, 1 μs long with amplitude 16 V, was generated by a HP8116 function generator. The receiving pinducers were connected to an Agilent Infiniium oscilloscope through a custom built multiplexing box followed by an AD8335 amplifier from Analog Devices. The sampling rate of the oscilloscope was set to 25 MHz. Due to the limited resolution of the oscilloscope (8 bits), the received edge reflections had to be saturated to get sufficient resolution of the weaker defect reflections. The received signal from each element was averaged 16 times. The direct signal from the transmitter to the array was removed before processing. Diagonal loading was applied to all MVBF results according to (12).

A comparison between the SBF and the MVBF can be seen in figure 14. Again, no apodization was applied on the SBF. The log scale is cut at −20 dB. The holes are well pronounced in the lower part of the images where their true positions are marked with white crosses, or where necessary arrows. The pit and the notch are seen close to 0° and at 180°, respectively.

6. Discussion

An examination of the results in figure 4 shows the advantage of using multiple transmitters over a single transmitter. The use of four subarrays is apparently the optimal choice of subarray size since it manages to decorrelate the signal and simultaneously yields a reasonable resolution with an effective array size of 4 × 4 elements. Increasing the number of

subarrays to nine leads to a significantly worse performance since the effective array size is reduced to only 3×3 elements. The multiple transmitter setup does not suffer from these drawbacks since the full array size can be utilized due to the decorrelation effect achieved by averaging over multiple transmitters instead of multiple subarrays.

The simulated results in figures 6–8 show that the MVBF can be very efficient in suppressing interfering modes. In terms of angular resolution, the MVBF clearly outperforms the SBF. As expected, the single row array completely failed to suppress the interfering mode, but with only a two-row array, the MVBF performed very well in suppressing the interfering mode. For the eight-row array, both approaches showed reasonable performance in mode suppression, although the MVBF offers much better resolution.

The mode converted signals in figure 8 proved to be more difficult to suppress and the SBF performed significantly worse in this case. From the point of view of the algorithm, mode conversion is no different from the non-converted case. However, in this case there are two interfering signals to suppress, the unconverted and the converted S_0 mode, which leads to poorer performance when only two rows are available.

From the simulated results of the plate inspection it is apparent that the MVBF approach performs much better than the DAS, especially in terms of resolution. For the 4×4 array in figure 10, the effects from edge and corner reflections of the S_0 mode can be clearly seen at 45° intervals for both the SBF and the MVBF, although the MVBF is much more efficient in suppressing these effects. In the ideal simulation environment, where there is no uncertainty about element positions or dispersion characteristics, even the 4×4 array using the MVBF outperforms the 8×8 array using SBF in terms of resolution. Because of the relatively small array sizes, the holes in pair B were not resolved in any of the simulation examples. However, the holes in pair C were resolved on all array sizes for the MVBF, and on the 6×6 and 8×8 arrays for the SBF, even though the distance between the holes in pair C was less than in pair B. This is simply because pair C are at different distances from the center of the array and are therefore resolved in time.

The false echo seen in the center of the lower right quadrant of all the simulated image results, except for figure 13, is due to multiple transmitter excitation. As discussed in section 4.3, the covariance matrices formed by each transmission do not cover the same interference environment. It can be seen in the images that the false echo is in approximately the same range as the other defects, which is the reason for its appearance. Figure 13 shows that using fewer transmitters for each estimation can reduce these problems, at the cost of increased signal cancelation. Furthermore, hole pair B was underestimated compared to the SBF, and also compared to the images in figures 10–12, where the full set of transmitters were used.

The experimental results in figure 14 were not as conclusive as the simulated results. The notch is shown with higher resolution using the MVBF. Fewer artifacts are seen overall, especially close to the holes. However, the MVBF gave lower amplitude estimates of the holes than the SBF. It is likely that the MVBF underestimated the amplitudes of the holes, which made the difference between the holes and the artifacts lower. Possible reasons could be signal cancelation due to the limited number of transmitters compared to the number of receivers, or steering vector errors. Steering vector errors could be caused by inaccuracies in the dispersion characteristics or errors in the array element positions. The pits are clearly seen using both methods. Hole pair C was not resolved using either method. It should be noted that an array with 7 mm element spacing was used for the experimental results, which allowed hole pair B to be resolved in the experimental data due to the increased array width. No aliasing effects were identified in the results due to the spatial undersampling of the A_0 mode.

The saturation of the edge reflections created a significant amount of noise in post-processed data from both algorithms in the areas closer than 100 mm to the edges, which is the reason for not showing images covering the whole plate. After increasing the amplitude range of the oscilloscope, and thereby avoiding saturation, these problems disappeared. Unfortunately, the insufficient dynamic range made the much weaker signals from the defects undetectable using either of the algorithms.

An obvious limitation of the measurement setup is the simultaneous use of only eight array elements, which hindered assessment of the potential effects of interelement scattering that may be encountered for a full 2D array.

7. Conclusions

The previously proposed adaptive approach for Lamb wave imaging [22] using a single transmitter has been extended to cover the multiple transmitter case. Multiple transmitter setups do not suffer from the drawbacks caused by the spatial smoothing preprocessing step required in single transmitter setups. The interfering mode suppression capabilities of the new MVBF approach was shown to outperform the SBF on simulated data. The simulated results showed that the resolution of the proposed approach is significantly better compared to the SBF, especially for small arrays. The approach also performed better than the SBF on experimental data.

Signal cancelation that may result in the underestimation of the signal amplitudes is an issue that needs to be addressed when working with the MVDR algorithm. Underestimation could be seen in the results for several defects. The implications of using multiple transmitters have been described and investigated. Using as many transmitters as there are receivers reduces the problem of signal cancelation. However, the results showed that the performance of the MVBF with regard to interferer cancelation can be reduced for certain cases when the number of transmitters are equal or close to the number of receivers and multiple scatterers are in the same range. A simple approach to mitigate such problems was proposed.

The proposed method can be used on non-homogeneous and anisotropic plates as long as accurate dispersion characteristics are available.

Acknowledgments

The authors would like to thank Mr Roman Klis for performing the measurements. This work was supported by SKB (the Swedish Nuclear Fuel and Waste Management Co.) in the project 1052/09.

References

[1] Mohr W and Höller P 1976 On inspection of thin-walled tubes for transverse and longitudinal flaws by guided ultrasonic waves *IEEE Trans. Son. Ultrason.* **23** 369–74
[2] Lehfeldt E and Höller P 1967 Lamb waves and lamination detection *Ultrasonics* **5** 255–7
[3] Wilcox P D, Lowe M J S and Cawley P 2000 Lamb and SH wave transducer arrays for the inspection of large areas of thick plates *Ann. Rev. Prog. QNDE* **19A** 1049–56
[4] Giurgiutiu V and Bao J 2002 Embedded ultrasonic structural radar for the nondestructive evaluation of thin-wall structures *Proc. 2002 ASME Int. Mechanical Engineering Congr.* paper 3901 pp 333–40
[5] Wilcox P D 2003 Omni-directional guided wave transducer arrays for the rapid inspection of large areas of plate structures *IEEE Trans. Ultrason. Ferroelectr. Freq. Control* **50** 699–709
[6] Fromme P, Wilcox P D, Lowe M J S and Cawley P 2006 On the development and testing of a guided ultrasonic wave array for structural integrity monitoring *IEEE Trans. Ultrason. Ferroelectr. Freq. Control* **53** 777–85
[7] Rajagopalan J, Balasubramaniam K and Krishnamurthy C V 2006 A phase reconstruction algorithm for Lamb wave based structural health monitoring of anisotropic multilayered composite plates *J. Acoust. Soc. Am.* **119** 872
[8] Yan F, Royer R L Jr and Rose J L 2010 Ultrasonic guided wave imaging techniques in structural health monitoring *J. Intell. Mater. Syst. Struct.* **21** 377
[9] Salas K I and Cesnik C E S 2009 Guided wave excitation by a clover transducer for structural health monitoring: theory and experiments *Smart Mater. Struct.* **18** 075005
[10] Wilcox P D, Lowe M and Cawley P 2005 Omnidirectional guided wave inspection of large metallic plate structures using an EMAT array *IEEE Trans. Ultrason. Ferroelectr. Freq. Control* **52** 653–65
[11] Giurgiutiu V 2005 Tuned lamb wave excitation and detection with piezoelectric wafer active sensors for structural health monitoring *J. Intell. Mater. Syst. Struct.* **16** 291–305
[12] Wilcox P D 2003 A rapid signal processing technique to remove the effect of dispersion from guided wave signals *IEEE Trans. Ultrason. Ferroelectr. Freq. Control* **50** 419–27
[13] Velichko A and Wilcox P D 2008 Guided wave arrays for high resolution inspection *J. Acoust. Soc. Am.* **123** 186–96
[14] Wang Z, Li J and Wu R 2005 Time-delay- and time-reversal-based robust capon beamformers for ultrasound imaging *IEEE Trans. Med. Imag.* **24** 1308–22
[15] Sasso M and Cohen-Bacrie C 2005 Medical ultrasound imaging using the fully adaptive beamformer *IEEE Int. Conf. on Acoustics, Speech and Signal Processing* vol 2, pp 489–92
[16] Synnevåg J F, Austeng A and Holm S 2007 Adaptive beamforming applied to medical ultrasound imaging *IEEE Trans. Ultrason. Ferroelectr. Freq. Control* **54** 1606–13
[17] Michaels J E, Hall J S and Michaels T E 2009 Adaptive imaging of damage from changes in guided wave signals recorded from spatially distributed arrays *Proc. SPIE* **7295** 729515
[18] Stepinski T and Engholm M 2008 On the development and testing of an uniform circular array for structural health monitoring of planar structures *Proc. Fourth European Workshop on Structural Health Monitoring (Krakow, July 2008)*
[19] Stepinski T and Engholm M 2009 Piezoelectric circular array for structural health monitoring using plate waves *7th Int. Workshop on Structural Health Monitoring (Stanford, CA, Sept. 2009)*
[20] Engholm M and Stepinski T 2010 Direction of arrival estimation of Lamb waves using circular arrays *Struct. Health Monit.* doi:10.1177/1475921710379512
[21] Engholm M 2010 Ultrasonic arrays for sensing and beamforming of Lamb waves *PhD Thesis* Uppsala University
[22] Engholm M and Stepinski T 2010 Adaptive beamforming for array imaging of plate structures using Lamb wave *IEEE Trans. Ultrason. Ferroelectr. Freq. Control* **57** 2712–24
[23] Rose J L 1999 *Ultrasonic Waves in Solid Media* (Cambridge: Cambridge University Press)
[24] Alleyne D and Cawley P 1991 A two-dimensional Fourier transform method for the measurement of propagating multimode signals *J. Acoust. Soc. Am.* **89** 1159–68
[25] Widrow B, Duvall K, Gooch R and Newman W 1982 Signal cancellation phenomena in adaptive antennas: causes and cures *IEEE Trans. Antennas Propag.* **30** 469–78
[26] Li J, Stoica P and Wang Z 2003 On robust capon beamforming and diagonal loading *IEEE Trans. Signal Process.* **51** 1702–15
[27] Krolik J and Swingler D 1989 Multiple broad-band source location using steered covariance matrices *IEEE Trans. Acoust. Speech Signal Process.* **37** 1481–94
[28] Hung H and Kaveh M 1988 Focussing matrices for coherent signal-subspace processing *IEEE Trans. Acoust. Speech Signal Process.* **36** 1272–81
[29] Shan T J, Wax M and Kailath T 1985 On spatial smoothing for directon-of-arrival estimation of coherent signals *IEEE Trans. Acoust. Speech Signal Process.* **33** 806–11
[30] Papazoglou M and Krolik J L 1996 High resolution adaptive beamforming for three-dimensional acoustic imaging of zooplankton *J. Acoust. Soc. Am.* **100** 3621–30